



Research Article

Systematic Investigation of Selected Bio-molecules Potentially Effective in Inhibiting SARS-CoV-2/COVID-19 via In-Silico Analysis

Akash Vanzara^{*ID}, Saloni Ambasan, Amit Shrivastav, Swati Patel, Vishal Patel, Hardik Soni, Vikram Trivedi

Vasu Research Center, Makarpura G.I.D.C, Makarpura, Vadodara, 390013, Gujarat, India
Email: akash@vasuresearch.com

Received: 2 January 2024; Revised: 7 April 2024; Accepted: 26 April 2024

Abstract: There have been millions of cases of Coronavirus, Severe acute respiratory syndrome coronavirus 2 (SARS-CoV-2) with high infectious properties during the year 2019. To counter the situation, certain medications were prescribed by health experts, such as Remdesivir, Dexamethasone, Azithromycin and Hydroxychloroquine, following the World Health Organization (WHO) guidelines. While vaccines have since been administered to alleviate symptoms, alternative treatments like Ayurvedic remedies are being explored. This study specifically delves into in-silico analysis using Autodock 4.2.6 software to assess selected phytomarkers against the 6LU7-main protease protein. The chemical structures of these drugs were analyzed using SWISSADME software to evaluate their drug-likeness properties. Molecular docking was conducted using Autodock tools 1.5.6, and receptor-ligand interactions were visualized using PyMol 2.3. Discovery Studio Visualizer 2020 generated a two-dimensional map illustrating bond interactions and distances between drugs and receptors. The mean binding energies of the compounds, including Nobiletin, Tangeretin, Sideroxylonal C, Coriandron, Epicatechin, Epigallocatechin gallate, Luteolin, Ombuin, Tamarixetin, 6-deacetylnimbin, Nimbolide, and Tricin were -5.66, -6.00, -6.46, -6.40, -6.91, -6.51, -6.34, -6.46, -6.99, -6.82, -6.51, -7.85, and -6.35 kcal/mol. Notably, several bioactive markers, including Nobiletin, Tangeretin, Epicatechin, Epigallocatechin gallate (EGCG), Ombuin, Tamarixetin, and Nimbolide, exhibited similar binding sites to synthetic drugs like Remdesivir, such as PHE140, CYS145, GLU166, and GLN189. The investigation also addresses Absorption, Distribution, Metabolism, Excretion, and Toxicity (ADMET) modelling, binding energy scores, and binding affinity, emphasizing the importance of vaccination as a crucial measure to curb the spread of infection.

Keywords: alternative medication, in-silico analysis, morden and phytochemical drug properties

1. Introduction

The end of 2019 saw a significant global outbreak caused by SARS-CoV-2, resulting in a major impact on the health sector. By July 7, 2022, a total of 550, 218, 992 cases had been confirmed, with 6, 343, 783 reported deaths.¹ The initial report of the disease emerged on December 30 in Wuhan, with 27 patients displaying pneumonia symptoms of unknown origin.²⁻³ Early stages of the illness presented varied respiratory symptoms among patients. To identify the unknown pathogen, samples were collected and sequenced, revealing a novel Coronavirus-2 (CoV-2).⁴⁻⁶ CoV-2,

categorized into alpha, beta, and gamma-CoV groups, exhibited distinct properties, such as gastrointestinal disorders for Alpha-CoV, and associations with bat coronaviruses, Middle East Respiratory Syndrome (MERS), and Severe Acute Respiratory Syndrome (SARS) for Beta-CoV.⁷⁻⁸

In response to the pandemic, rapid vaccination campaigns emerged as crucial tools in safeguarding public health and preventing further spread. Additionally, pharmaceutical interventions like Dexamethasone, a glucocorticoid with anti-inflammatory and immunosuppressive effects, were prescribed.⁹⁻¹¹ Remdesivir, initially effective against Ebola, showed promise against COVID-19, with studies indicating faster recovery times and lower mortality rates compared to placebos.¹²⁻¹³ Remdesivir, functioning as a nucleotide prodrug akin to an adenosine analog, binds to the viral Ribonucleic acid (RNA)-dependent RNA polymerase, thereby hindering viral replication through premature termination of RNA transcription. Its efficacy against SARS-CoV-2 has been evidenced both in vitro and in vivo. Intravenous administration of remdesivir is Food and Drug Administration (FDA) approved for treating COVID-19 in adults and pediatric patients aged ≥ 28 days, weighing ≥ 3 kg. For non-hospitalized individuals with mild to moderate COVID-19 and at high risk of progressing to severe illness, initiation of remdesivir within 7 days of symptom onset and a 3-day course is recommended. Hospitalized patients should receive remdesivir for 5 days or until discharge.¹⁴ Hydroxychloroquine and Azithromycin were also explored in combination therapies, showing reductions in hazard ratios.¹⁵⁻¹⁸ Alongside these pharmaceuticals, there's recognition of the importance of natural therapies, harnessing bioactive compounds with immunomodulatory, anti-inflammatory, and antiviral properties.¹⁹⁻²³

In this study, twelve bioactive molecules, including Nobiletin, Tangeretin, and Epicatechin, were screened for their medicinal potential. Through in silico analysis and assessment of pharmacokinetic attributes using artificial intelligence-based software, their interactions with SARS-CoV-2 were explored, alongside considerations of Absorption, Distribution, Metabolism, Excretion, and Toxicity (ADMET).²⁴

2. Materials and methods

2.1 Systematic screening of macromolecules

2.1.1 The virtual screening

A crystallographic structure of SARS-CoV-2 Main Protease (M^{pro}) with an additional N3 inhibitor was used to screen macromolecules.²⁴ CoV-2 Structure was derived from RCSB Protein Data Bank (PDB) (Deposited: 26-01-2020; Released: 05-02-2020) and prepared for computation by using Autodock 4.2.6. The homodimer virus protein consists of two chains, A and C, of which the chain A macromolecule was prepared for computational analysis.

2.1.2 Drug and ligand computing

The three-dimensional structures of various drugs, including Remdesivir (CID 121304016), Nobiletin (CID 72344), Tangeretin (CID 68077), Sideroxylylonal C (CID 10413640), Coriandrone-A (CID 131752231), Epicatechin (CID 72276), Epigallocatechin gallate (CID 65064), Luteolin (CID 5280445), Ombuin (CID 5320287), Tamarixetin (CID 5281699), 6-Deacetylnimbin (CID 10505484), Nimbolide (CID 100017), and Tricin (CID 5281702), were sourced from the PubChem database in .sdf format files. Additionally, all selected compounds were subjected to Lipinski's rules of 5 to assess their drug-likeness properties.²⁵ The SWISSADME predictive online software was utilized for this evaluation, with specific criteria including the acceptance of 10 hydrogen bond acceptors, no more than 5 hydrogen bond donors, a molecular weight range of 160-500 g/mol, and a logP value between -0.4 and 5.6.²⁶

2.1.3 Active amino acid site ascertainment

Previous research on SARS-CoV-2 identified active amino acid residues, which were subsequently analyzed using UCSF Chimera (version 1.14) and Biovia Discovery Studio 2020. The identified active amino acid sites of the virus include THR 24, THR 26, PHE140, ASN 142, GLY143, CYS145, HIS163, HIS164, GLU166, HIS 172, GLN189, and THR190.²⁷⁻³¹ Further analysis involved examining these amino acid residues within grids positioned at X: 50, Y: 44, Z: 58 and X: -14.793, Y: 15.563, Z: 70.843, with a spacing of 0.575. The parameters were saved in .grid file format, and the final output file was generated in .gpf format.

2.1.4 Molecular docking

The flexibility of ligand and receptor protein molecules was assessed using Autodock tools 1.5.6. Initially, the .sdf file format was converted to .pdb format files using Open Babel GUI 3.0 software.³² Subsequently, receptor optimization was conducted by eliminating excess water molecules and hetatm, while ensuring hydrogen atoms and Kollman charges grid parameters were set according to the active sites coordinates. Molecular docking was then performed using a genetic algorithm (GA) with 1,750,000 generations using Autodock tools. The top ten docking hits were selected based on average binding energy. To elucidate receptor-ligand interactions, PyMol 2.3 was employed to analyze the docking site and position.³³ Additionally, a two-dimensional map was generated using Discovery Studio Visualizer 2020 to further comprehend the interactions.

2.1.5 Pharmacokinetic predictive studies

A pharmacokinetic study was conducted utilizing the pkCSM server to assess ADMET. The Open Babel 3.0 software was employed to convert the ligand's .sdf file into a SMILES file.³⁴

3. Results

3.1 Drug likeness properties

The drug-likeness properties of several compounds, including Nobiletin, Tangeretin, Sideroxydonal C, Coriandron, Epicatechin, Epigallocatechin gallate, Luteolin, Ombuin, Tamarixetin, 6-Deacetylnimbin, Nimbolide, and Tricin, were evaluated using Lipinski rules (Table 1). Most of these compounds showed adherence to Lipinski rules, with zero violations, except for Epigallocatechin gallate, which had two violations. Specifically, Remdesivir exhibited two violations, exceeding the limit for hydrogen-bond acceptors and having a molecular weight of 602.58 g/mol, with a lipophilicity of Log Po/w 1.53. Nobiletin had a lipophilicity of 3.02, with 8 hydrogen-bond acceptors and a molecular weight of 402.39 g/mol. Tangeretin showed no violations, with a molecular weight of 372.37 g/mol, 14 hydrogen-bond acceptors, and a lipophilicity of 2.04. Sideroxydonal C had one violation due to its 10 hydrogen-bond acceptors and 5 hydrogen-bond donors, with a lipophilicity of 2.81 and a molecular weight of 500.5 g/mol. Coriandron-A exhibited no violations, with a molecular weight of 292.33 g/mol and a lipophilicity of 2.25, along with 5 hydrogen-bond acceptors and 1 hydrogen-bond donor. Epicatechin also had no violations, with a molecular weight of 290.27 g/mol, a lipophilicity of 0.85, and 6 hydrogen-bond acceptors and 5 hydrogen-bond donors. Epigallocatechin gallate, however, showed two violations, with 11 hydrogen-bond acceptors, 8 hydrogen-bond donors, and a lipophilicity of 0.95, at a molecular weight of 458.37 g/mol. Luteolin exhibited zero violations, with a lipophilicity of 1.73, 6 hydrogen-bond acceptors, 4 hydrogen-bond donors, and a molecular weight of 286.2 g/mol. Ombuin showed no violations, with a molecular weight of 330.29 g/mol, a lipophilicity of 2.25, 7 hydrogen-bond acceptors, and 3 hydrogen-bond donors. Similarly, Tamarixetin demonstrated zero violations, with a molecular weight of 316.26 g/mol, a lipophilicity of 1.85, 7 hydrogen-bond acceptors, and 4 hydrogen-bond donors. 6-Deacetylnimbin also showed zero violations, with a lipophilicity of 2.75, 8 hydrogen-bond acceptors, and 1 hydrogen-bond donor. Likewise, Nimbolide exhibited zero violations, with a molecular weight of 466.52 g/mol, a lipophilicity of 3.11, and 7 hydrogen-bond acceptors.

Table 1. Pharmacokinetic study of Nobiletin, Tangeretin, Sideroxydonal C, Coriandron, Epicatechin, Epigallocatechin gallate, Luteolin, Ombuin, Tamarixetin, 6-Deacetylumbin, Nimbolide, Tricin by using Lipinski rules of five

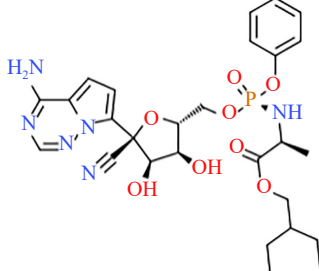
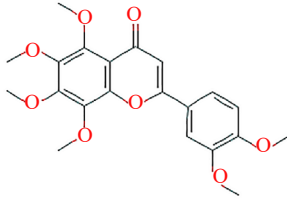
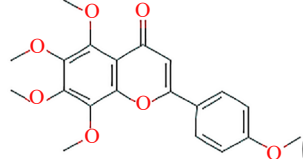
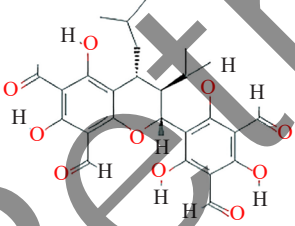
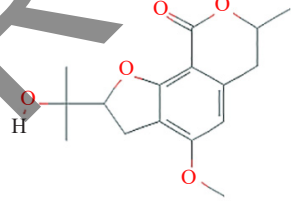
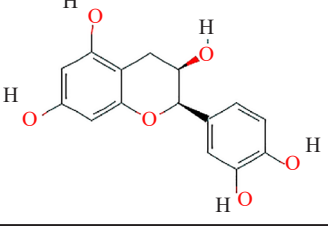
Sr. No.	Name of compound	Structure	Molecular formula	Lipinski rules of five	
				Properties	Value
1	Remdesivir		$C_{22}H_{29}FO_9$	Molecular weight (< 500 g/mol)	602.58 g/mol
				LogP (< 5)	1.53
				H-Bond donor (< 5)	4
				H-Bond acceptor (< 10)	12
				Violation	2
2	Nobiletin		$C_{21}H_{22}O_8$	Molecular weight (< 500 g/mol)	402.4 g/mol
				LogP (< 5)	3.02
				H-Bond donor (< 5)	0
				H-Bond acceptor (< 10)	8
				Violation	0
3	Tangeretin		$C_{20}H_{20}O_7$	Molecular weight (< 500 g/mol)	372.4 g/mol
				LogP (< 5)	3.02
				H-Bond donor (< 5)	0
				H-Bond acceptor (< 10)	7
				Violation	0
4	Sideroxydonal C		$C_{26}H_{28}O_{10}$	Molecular weight (< 500 g/mol)	500.5 g/mol
				LogP (< 5)	2.81
				H-Bond donor (< 5)	5
				H-Bond acceptor (< 10)	10
				Violation	1
5	Coriandron-A		$C_{16}H_{20}O_5$	Molecular weight (< 500 g/mol)	292.33 g/mol
				LogP (< 5)	2.25
				H-Bond donor (< 5)	1
				H-Bond acceptor (< 10)	5
				Violation	0
6	Epicatechin		$C_{15}H_{14}O_6$	Molecular weight (< 500 g/mol)	290.27 g/mol
				LogP (< 5)	0.85
				H-Bond donor (< 5)	5
				H-Bond acceptor (< 10)	6
				Violation	0

Table 1. (cont.)

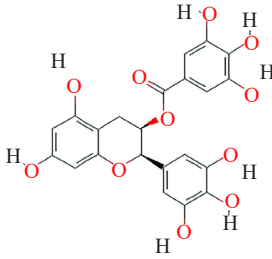
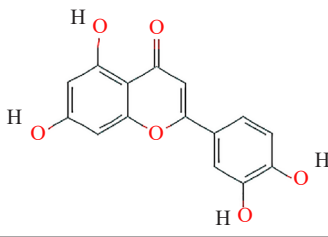
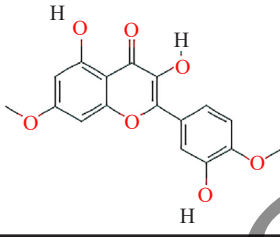
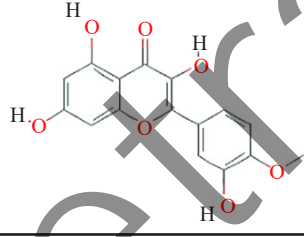
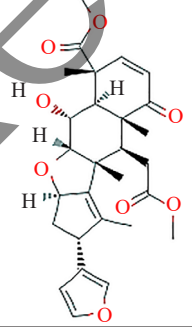
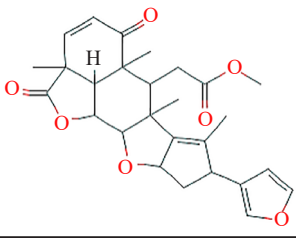
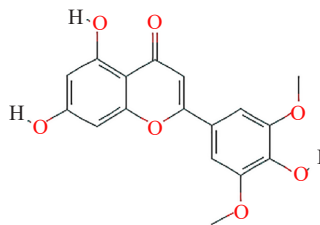
Sr. No.	Name of compound	Structure	Molecular formula	Lipinski rules of five	
				Properties	Value
7	Epigallocatechin gallate		$C_{22}H_{18}O_{11}$	Molecular weight (< 500 g/mol)	458.37 g/mol
				LogP (< 5)	0.95
				H-Bond donor (< 5)	8
				H-Bond acceptor (< 10)	11
				Violation	2
8	Luteolin		$C_{15}H_{10}O_6$	Molecular weight (< 500 g/mol)	286.2 g/mol
				LogP (< 5)	1.73
				H-Bond donor (< 5)	4
				H-Bond acceptor (< 10)	6
				Violation	0
9	Ombuin		$C_{17}H_{14}O_7$	Molecular weight (< 500 g/mol)	330.29 g/mol
				LogP (< 5)	2.25
				H-Bond donor (< 5)	3
				H-Bond acceptor (< 10)	7
				Violation	0
10	Tamarixetin		$C_{17}H_{14}O_7$	Molecular weight (< 500 g/mol)	316.26 g/mol
				LogP (< 5)	1.85
				H-Bond donor (< 5)	4
				H-Bond acceptor (< 10)	7
				Violation	0
11	6-Deacetylnimbin		$C_{28}H_{34}O_8$	Molecular weight (< 500 g/mol)	498.6 g/mol
				LogP (< 5)	2.75
				H-Bond donor (< 5)	1
				H-Bond acceptor (< 10)	8
				Violation	0
12	Nimbolide		$C_{27}H_{30}O_7$	Molecular weight (< 500 g/mol)	466.52 g/mol
				LogP (< 5)	3.11
				H-Bond donor (< 5)	0
				H-Bond acceptor (< 10)	7
				Violation	0

Table 1. (cont.)

Sr. No.	Name of compound	Structure	Molecular formula	Lipinski rules of five	
				Properties	Value
13	Tricin		C ₂₇ H ₃₀ O ₇	Molecular weight (< 500 g/mol)	330.29 g/mol
				LogP (< 5)	2.15
				H-Bond donor (< 5)	3
				H-Bond acceptor (< 10)	7
				Violation	0

3.1.1 Drug-receptor interactive binding energy and active site interlinkage

Table 2 presents the binding energies of various drugs. The lowest binding energies for Remdesivir, Nobiletin, Tangeretin, Sideroxylonal C, Coriandron, Epicatechin, Epigallocatechin gallate, Luteolin, Ombuin, Tamarixetin, 6-Deacetylnimbin, Nimbolide, and Tricin were found to be -5.66, -6.11, -6.46, -6.40, -6.96, -6.66, -7.06, -6.53, -7.09, -6.82, -6.94, -8.00, and -6.38 kcal/mol, respectively. Correspondingly, the mean binding energies were -5.66, -6.00, -6.46, -6.40, -6.91, -6.51, -6.34, -6.46, -6.99, -6.82, -6.51, -7.85, and -6.35 kcal/mol. Notably, among all drugs, Nimbolide exhibited the highest docking score with the lowest binding energy value of -8.00 kcal/mol, whereas its mean binding energy was -7.85 kcal/mol. Conversely, Remdesivir showed the same score of -5.66 kcal/mol for both lowest and mean binding energies.

Table 2. Binding energy, active site properties of of Nobiletin, Tangeretin, Sideroxylonal C, Coriandron, Epicatechin, Epigallocatechin gallate, Luteolin, Ombuin, Tamarixetin, 6-Deacetylnimbin, Nimbolide, Tricin against CoV-2

Sr. No.	Name of plant	Name of compound	Lowest binding energy kcal/mol	Mean binding energy kcal/mol	Amino acid binding sites
1	Synthetic drug	Remdesivir	-5.66	-5.66	PHE140, CYS145, GLU166, GLN189
		Nobiletin	-6.11	-6.00	ASN142, GLY143, CYS145, HIS163, GLU166, GLN189, THR190
2	<i>Citrus sinensis</i>	Tangeretin	-6.46	-6.46	GLY143, CYS145, HIS163, HIS164, GLU166, GLN189
3	<i>Eucalyptus globulus</i>	Sideroxylonal C	-6.40	-6.40	PHE140, ASN142, CYS145, HIS163, GLU166
4	<i>Coriandrum sativum</i>	Coriandron-A	-6.96	-6.91	PHE140, GLY143, CYS145, HIS163, GLU166, HIS172
5	<i>Camellia sinensis</i>	Epicatechin	-6.66	-6.51	CYS145, HIS163, HIS164, GLU166, GLN189
		Epigallocatechin gallate	-7.06	-6.34	THR26, GLY143, CYS145, HIS163, GLU166, GLN189
6	<i>Lavandula stoechas</i>	Luteolin	-6.53	-6.46	THR26, GLY143, CYS145, HIS163, GLU166
		Ombuin	-7.09	-6.99	PHE140, GLY143, CYS145, HIS163, GLU166
7	<i>Syzygium aromaticum</i>	Tamarixetin	-6.82	-6.82	PHE140, ASN142, HIS163, GLU166, GLN189
		6-Deacetylnimbin	-6.94	-6.51	HIS163, GLU166, HIS172, GLN189
8	<i>Azadirachta indica</i>	Nimbolide	-8.00	-7.85	PHE140, ASN142, GLY143, CYS145, HIS163, GLU166
		Tricin	-6.38	-6.35	ASN142, CYS145, HIS163, GLU166, THR190

Figure 1 illustrates the typical receptor-ligand interaction for the synthetic drug Remdesivir and as per the identified active amino acid sites of the virus.²⁷⁻³¹ It interacts with conventional hydrogen bonds involving PHE140, CYS145, GLN189, and GLU166, with bond distances noted as 2.17, 3.50, 2.34, and 2.69 Å, respectively. Additionally, it forms a carbon-hydrogen bond with ASN142, with a bond distance of 3.37 Å.

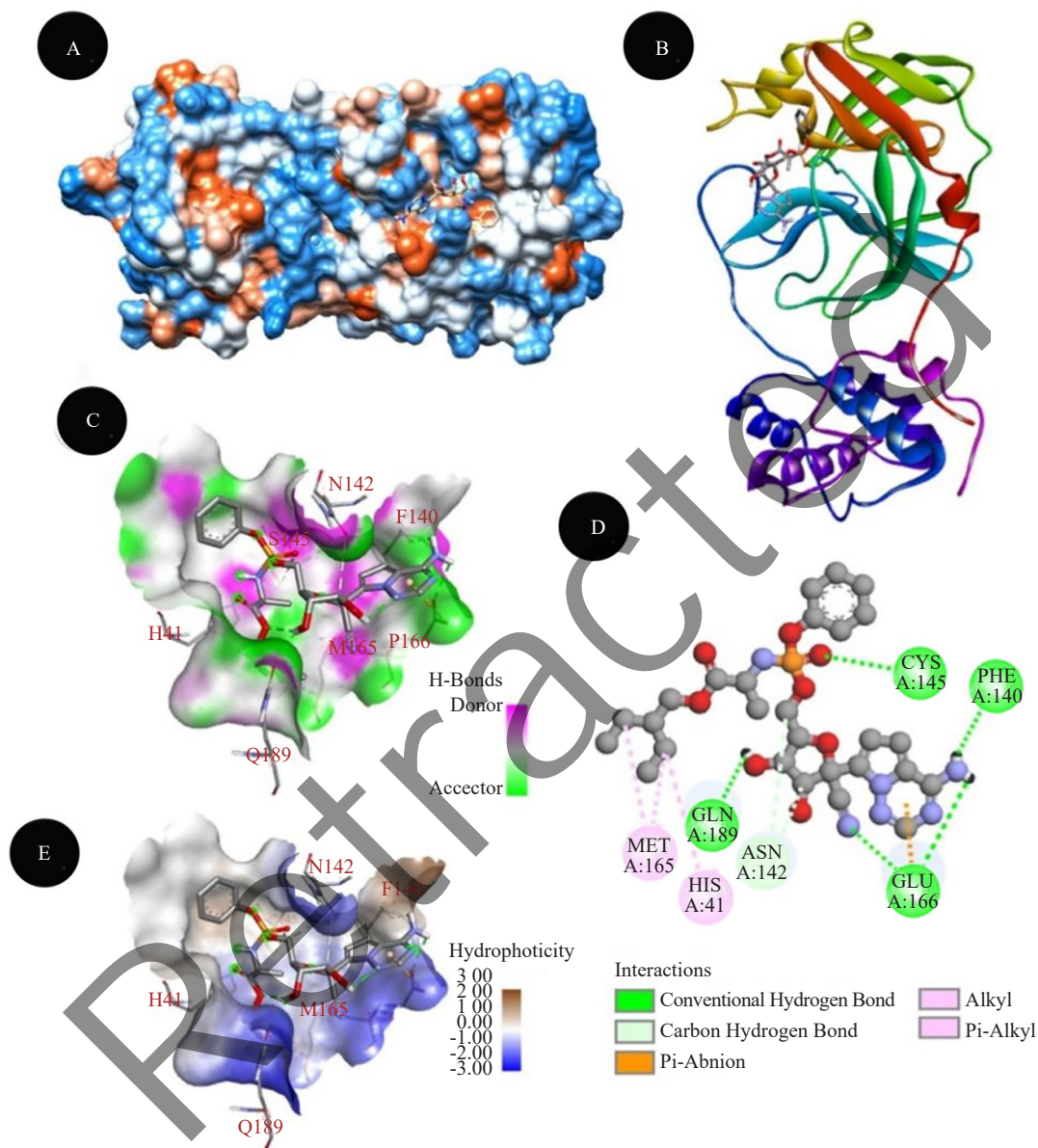


Figure 1. Docking analysis of SARS-CoV-2 M^{pro} binding with Remdesivir (A) hydrophobicity surface 3D representation (B) 3D representation of Remdesivir -SARS-CoV-2 M^{pro} interactions (C) Interactions of Remdesivir through H-bond in a pocket site of SARS-CoV-2 M^{pro} (D) 2D representation of Remdesivir in active site of SARS-CoV-2 M^{pro} (E) Interactions of Remdesivir through hydrophobic bond in a pocket site of SARS-CoV-2 M^{pro}

Similarly, Figures 2 & 3 illustrate Nobiletin & Tangeretin, which show similar bond patterns with a conventional hydrogen bond with the receptor GLU166, with a bond distance of 3.35 Å and 3.85 Å, and carbon-hydrogen bond with ASN142, with 2.22 Å and 3.07 Å. It also forms pi-alkyl bonds with CYS145 and HIS163, with a bond distance of 5.00 Å, 3.51 Å, 2.22 Å, and 3.71 Å, respectively.

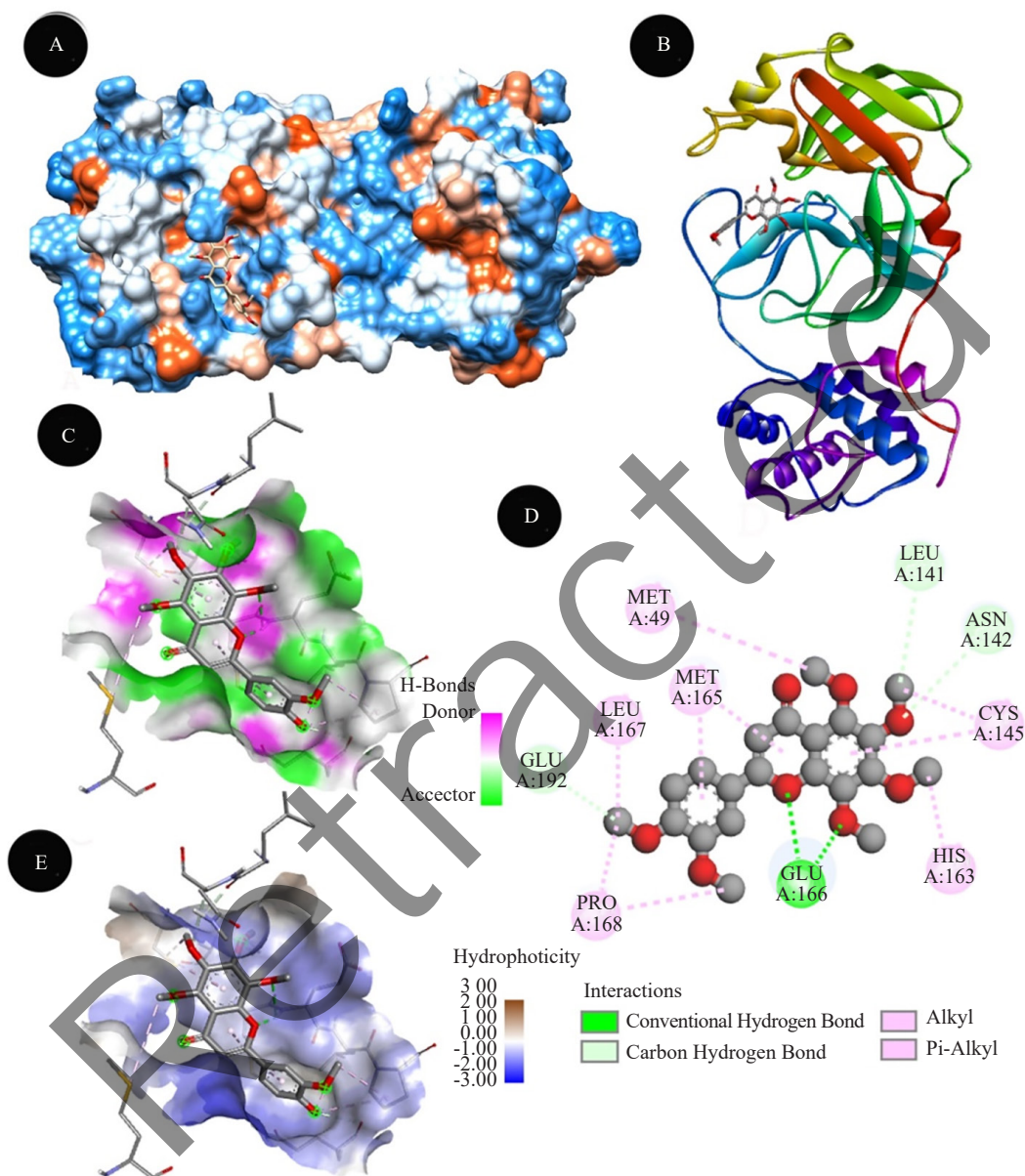


Figure 2. Docking analysis of SARS-CoV-2 M^{pro} binding with Nobiletin (A) hydrophobicity surface 3D representation (B) 3D representation of Nobiletin -SARS-CoV-2 M^{pro} interactions (C) Interactions of Nobiletin through H-bond in a pocket site of SARS-CoV-2 M^{pro} (D) 2D representation of Nobiletin in active site of SARS-CoV-2 M^{pro} (E) Interactions of Nobiletin through hydrophobic bond in a pocket site of SARS-CoV-2 M^{pro}

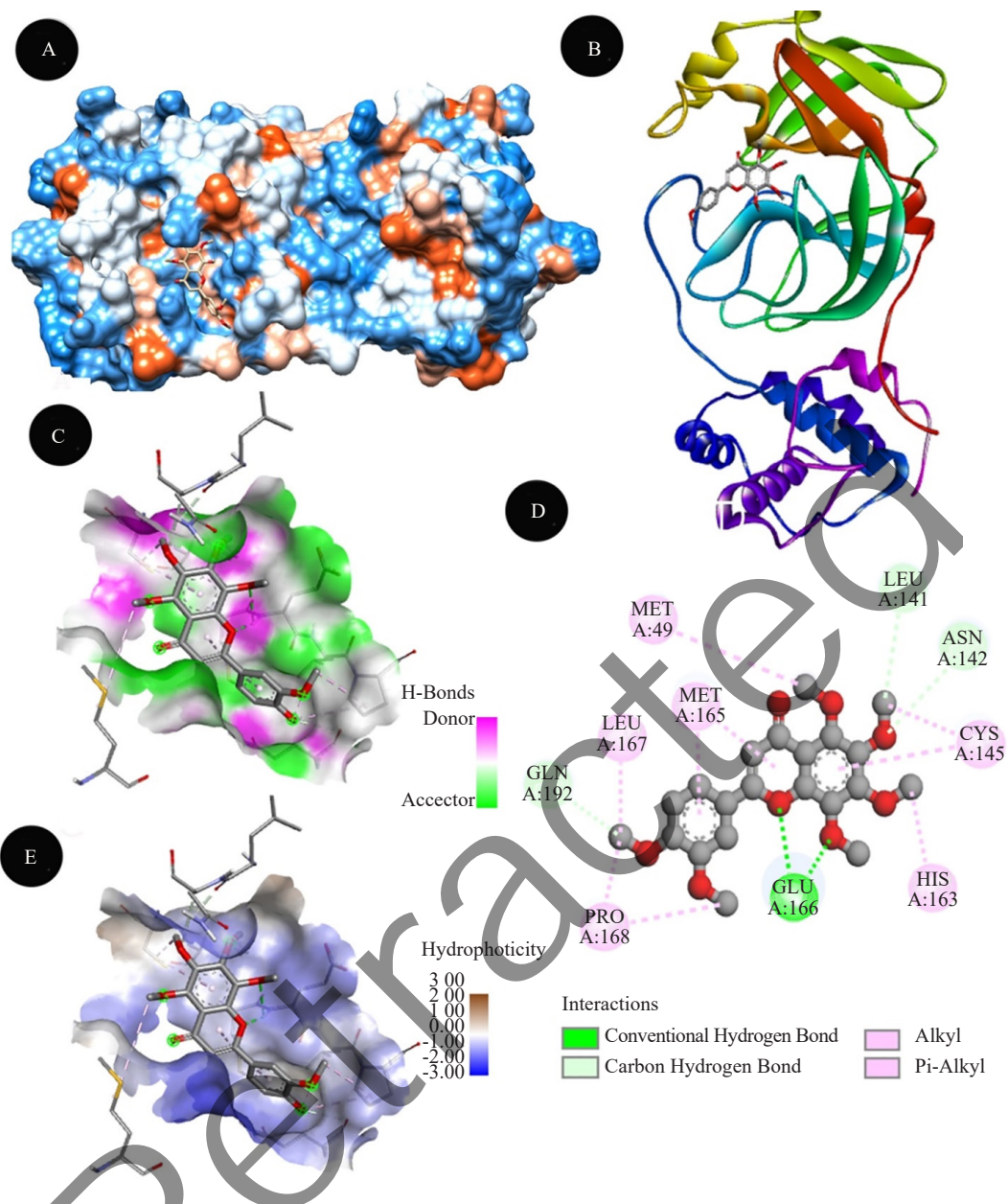


Figure 3. Docking analysis of SARS-CoV-2 M^{pro} binding with Tangeretin (A) hydrophobicity surface 3D representation (B) 3D representation of Tangeretin -SARS-CoV-2 M^{pro} interactions (C) Interactions of Tangeretin through H-bond in a pocket site of SARS-CoV-2 M^{pro} (D) 2D representation of Tangeretin in active site of SARS-CoV-2 M^{pro} (E) Interactions of Tangeretin through hydrophobic bond in a pocket site of SARS-CoV-2 M^{pro}

Furthermore, Figure 4 demonstrates Sideroxylylonal C, which exhibits various bond interlinkages, including three conventional hydrogen bonds with PHE140, ASN142, HIS163, and GLU166 receptors, with bond distances of 2.12 Å, 2.22 Å, 3.06 Å, and 3.10 Å, respectively. Additionally, it forms a pi-alkyl bond with the CYS145 receptor, with a distance of 4.61 Å.

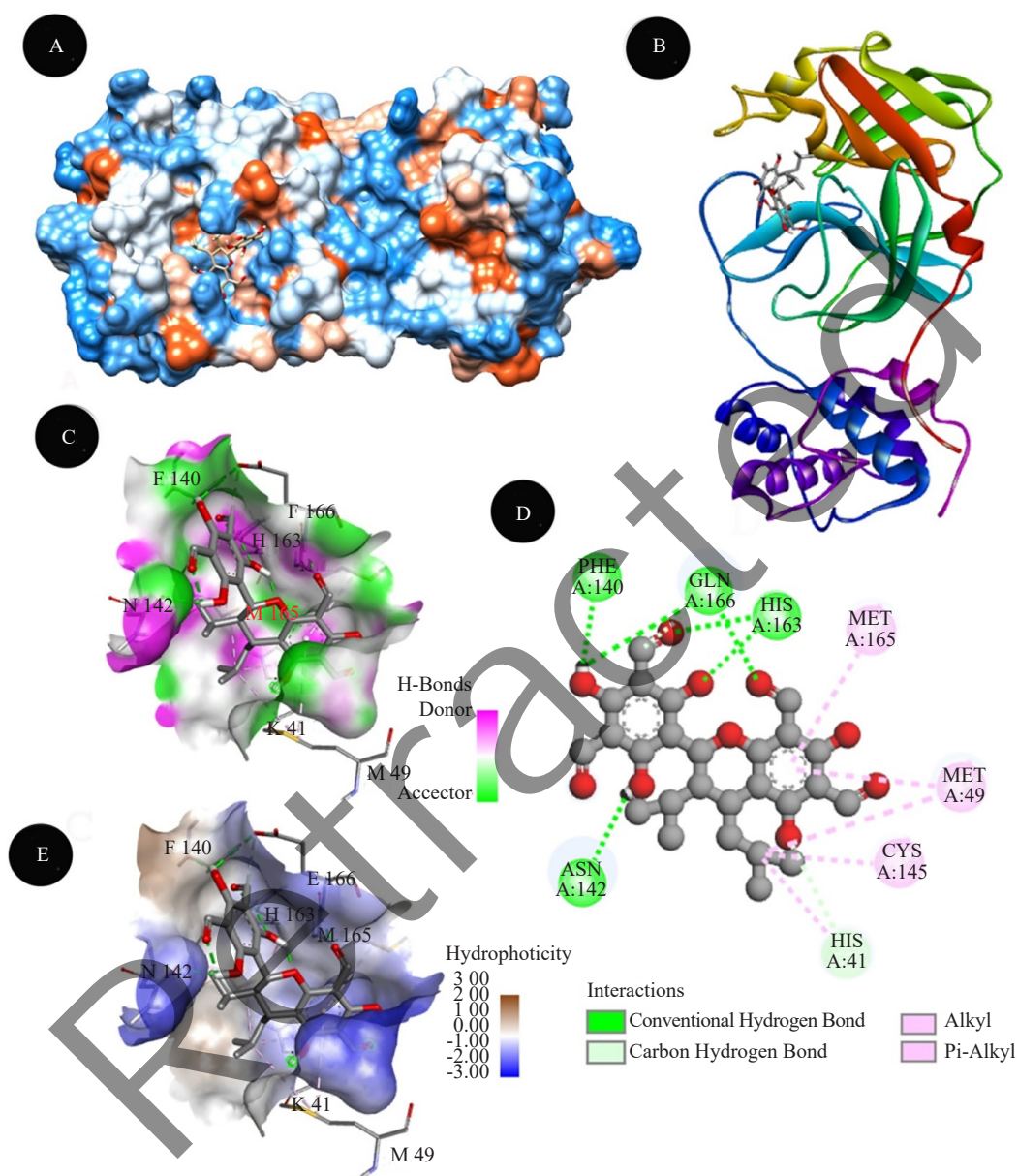


Figure 4. Docking analysis of SARS-CoV-2 M^{pro} binding with Sideroxylylonal C (A) hydrophobicity surface 3D representation (B) 3D representation of Sideroxylylonal C -SARS-CoV-2 M^{pro} interaction (C) Interactions of Sideroxylylonal C through H-bond in a pocket site of SARS-CoV-2 M^{pro} (D) 2D representation of Sideroxylylonal C in active site of SARS-CoV-2 M^{pro} (E) Interactions of Sideroxylylonal C through hydrophobic bond in a pocket site of SARS-CoV-2 M^{pro}

While, Figure 5 includes Coriandron-A which is involved in three conventional hydrogen bonds with GLY143, HIS163, and GLU166 receptors, with bond distances of 2.17 Å, 2.13 Å, and 2.60 Å, respectively. It also forms pi-alkyl bonds with PHE140 and HIS172 receptors, with bond distances of 5.47 Å and 5.37 Å, respectively, as well as a carbon-hydrogen bond with the CYS145 receptor, with a bond length of 3.55 Å.

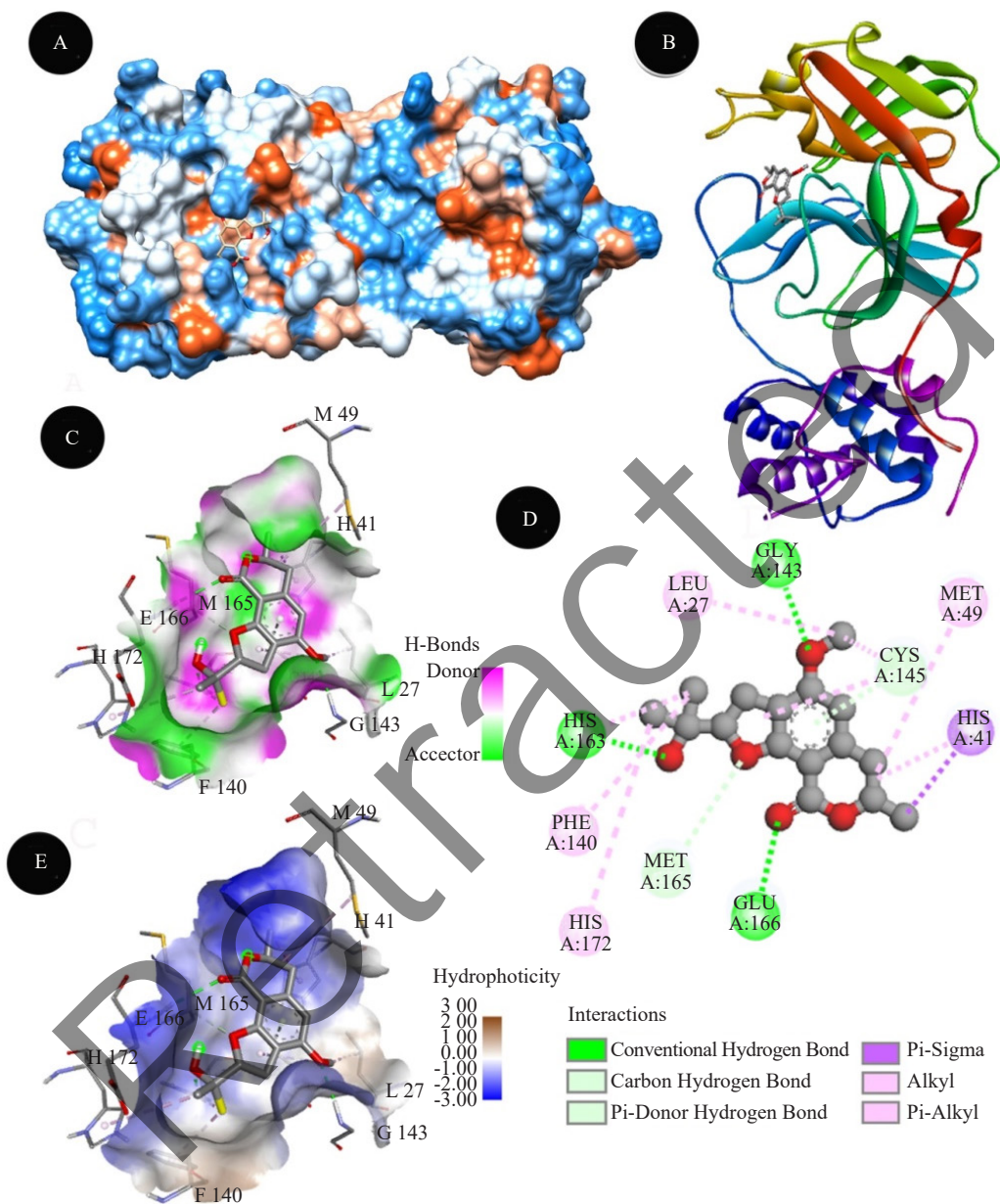


Figure 5. Docking analysis of SARS-CoV-2 M^{pro} binding with Coriandron-A (A) hydrophobicity surface 3D representation (B) 3D representation of Coriandron-A with SARS-CoV-2 M^{pro} interaction (C) Interactions of Coriandron-A through H-bond in a pocket site of SARS-CoV-2 M^{pro} (D) 2D representation of Coriandron-A in active site of SARS-CoV-2 M^{pro} (E) Interactions of Coriandron-A through hydrophobic bond in a pocket site of SARS-CoV-2 M^{pro}

In Figure 6, Epicatechin is involved with three conventional hydrogen bonds with HIS163, HIS164, and GLU166 receptors, with bond lengths of 2.06 Å, 2.14 Å, and 2.57 Å, respectively, along with a pi-sigma bond interaction with the GLN189 receptor, with a bond distance of 3.79 Å. Additionally, it forms a carbon-hydrogen bond with the CYS145 receptor, with a bond length of 4.01 Å.

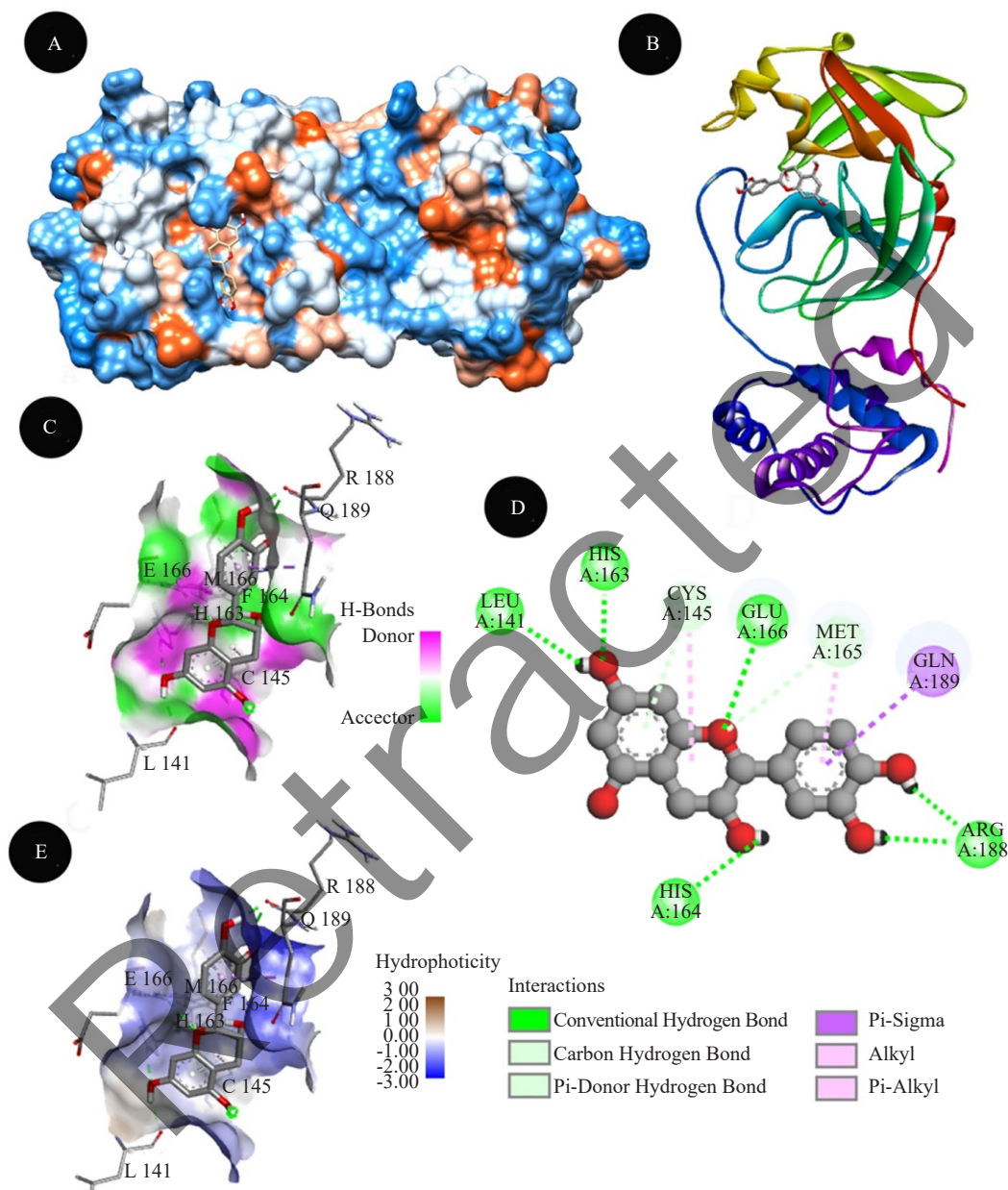


Figure 6. Docking analysis of SARS-CoV-2 M^{pro} binding with Epicatechin (A) hydrophobicity surface 3D representation (B) 3D representation of Epicatechin with SARS-CoV-2 M^{pro} interaction (C) Interactions of Epicatechin through H-bond in a pocket site of SARS-CoV-2 M^{pro} (D) 2D representation of Epicatechin in active site of SARS-CoV-2 M^{pro} (E) Interactions of Epicatechin through hydrophobic bond in a pocket site of SARS-CoV-2 M^{pro}

Figure 7 illustrates Epigallocatechin gallate, which forms five conventional bonds with receptors, including THR26, GLY143, HIS163, GLU166, and GLN189, with bond lengths of 1.94 Å, 1.96 Å, 1.69 Å, 2.49 Å, and 3.00 Å, respectively.

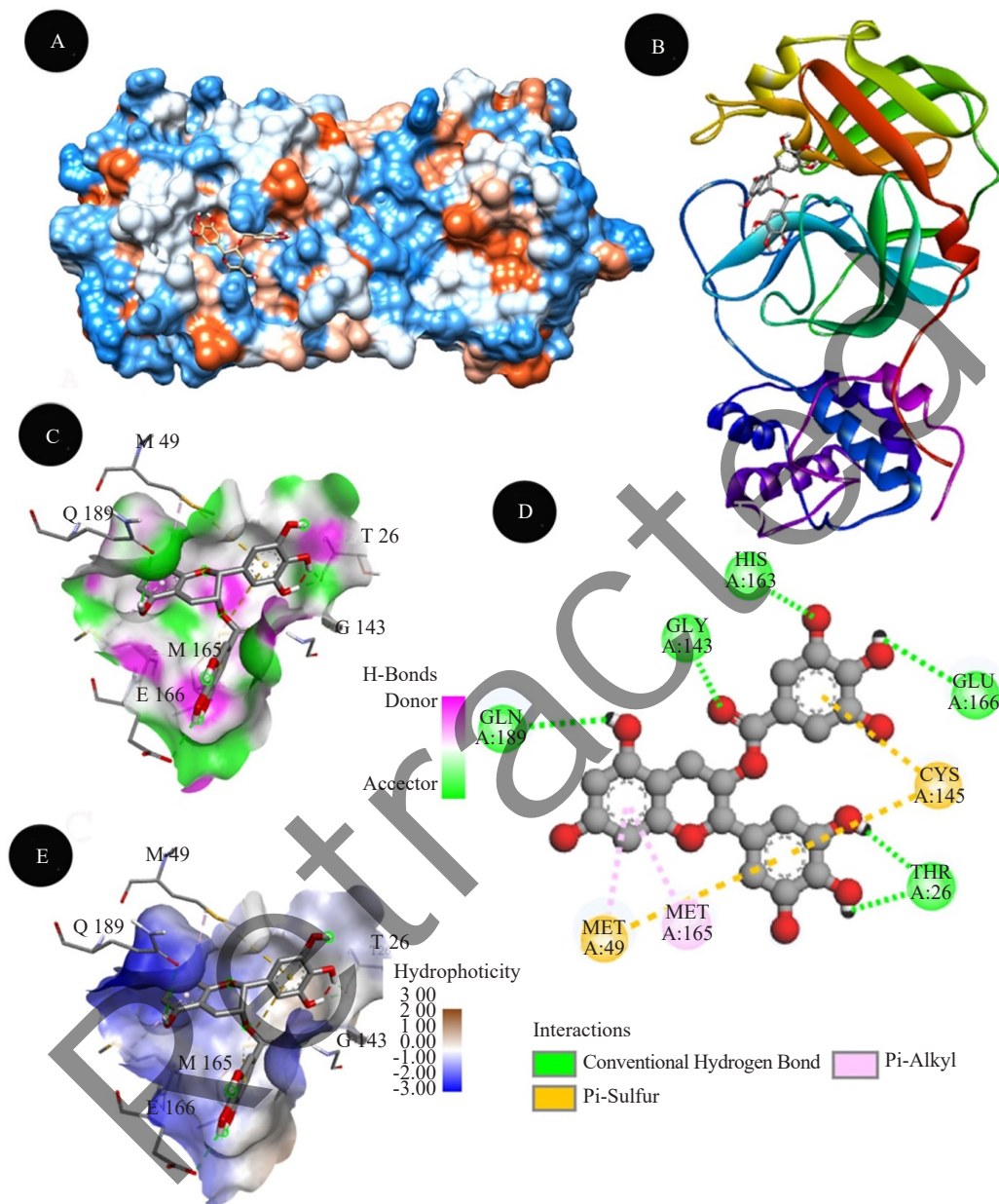


Figure 7. Docking analysis of SARS-CoV-2 M^{pro} binding with Epigallocatechin gallate (A) hydrophobicity surface 3D representation (B) 3D representation of Epigallocatechin gallate with SARS-CoV-2 M^{pro} interaction (C) Interactions of Epigallocatechin gallate through H-bond in a pocket site of SARS-CoV-2 M^{pro} (D) 2D representation of Epigallocatechin gallate in active site of SARS-CoV-2 M^{pro} (E) Interactions of Epigallocatechin gallate through hydrophobic bond in a pocket site of SARS-CoV-2 M^{pro}

Similarly, Luteolin in Figure 8 interacts with four conventional hydrogen bonds with THR26, GLY143, HIS163, and GLU166 receptors, and forms a carbon hydrogen bond with the CYS145 active amino acid residual site, with a bond length of 3.94 Å.

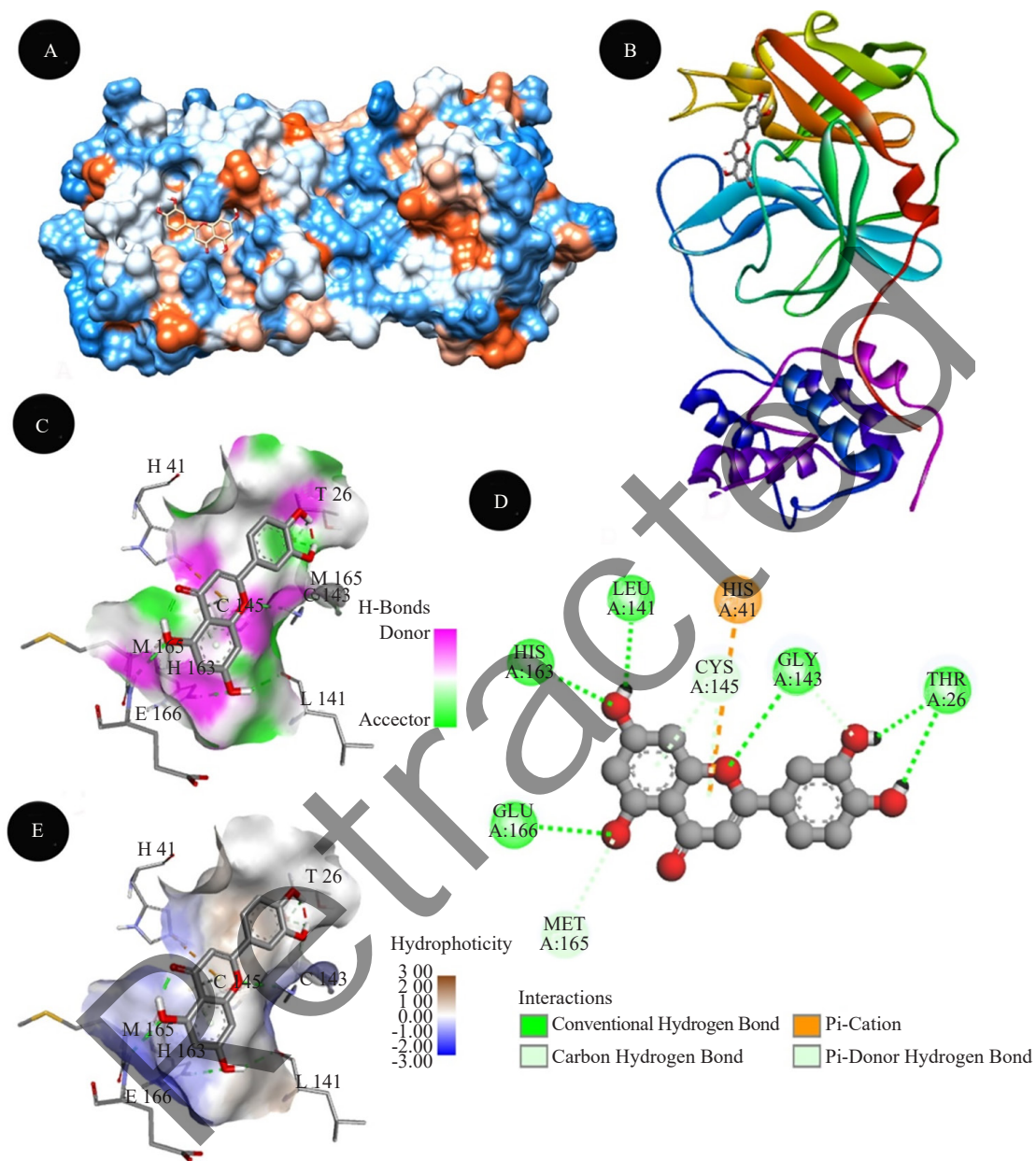


Figure 8. Docking analysis of SARS-CoV-2 M^{pro} binding with Luteolin (A) hydrophobicity surface 3D representation (B) 3D representation of Luteolin with SARS-CoV-2 M^{pro} interaction (C) Interactions of Luteolin through H-bond in a pocket site of SARS-CoV-2 M^{pro} (D) 2D representation of Luteolin in active site of SARS-CoV-2 M^{pro} (E) Interactions of Luteolin through hydrophobic bond in a pocket site of SARS-CoV-2 M^{pro}

While, Figure 9 demonstrates Ombuin, which forms a conventional hydrogen bond interaction with the GLY143 residual site, with a bond length of 2.78 Å. Additionally, it forms carbon-hydrogen bonds with the PHE140, CYS145, and GLU166 receptors, with bond lengths of 3.23 Å, 3.32 Å, and 3.26 Å, respectively, as well as pi-alkyl interactions with HIS163 and HIS172 receptors, with bond lengths of 5.26 Å and 4.98 Å, respectively.

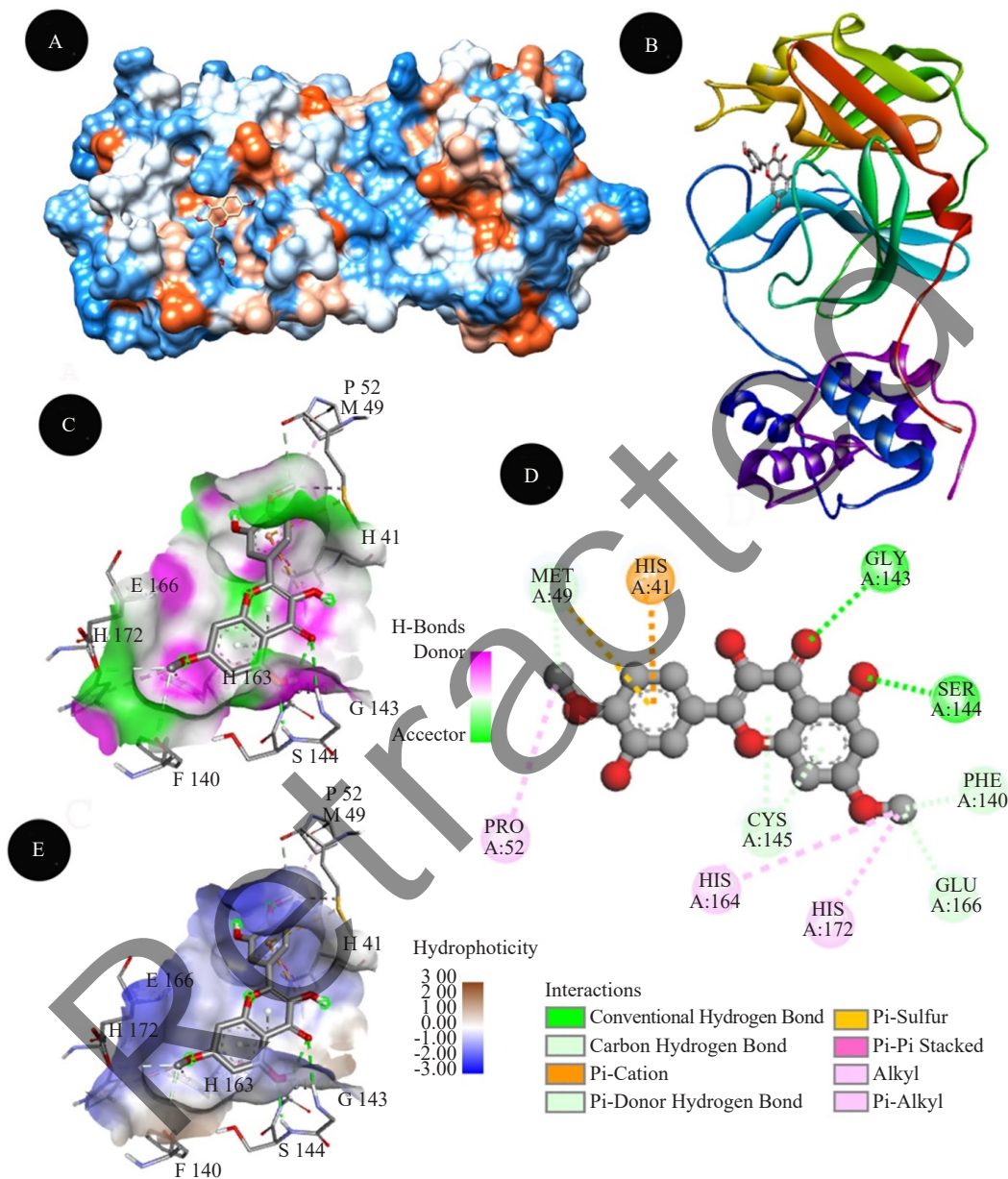


Figure 9. Docking analysis of SARS-CoV-2 M^{pro} binding with Ombuin (A) hydrophobicity surface 3D representation (B) 3D representation of Ombuin with SARS-CoV-2 M^{pro} interaction (C) Interactions of Ombuin through H-bond in a pocket site of SARS-CoV-2 M^{pro} (D) 2D representation of Ombuin in active site of SARS-CoV-2 M^{pro} (E) Interactions of Ombuin through hydrophobic bond in a pocket site of SARS-CoV-2 M^{pro}

Furthermore, Figure 10 is involved with Tamarixetin, which exhibits a similar bond pattern to Remdesivir, with four conventional hydrogen bonds with PHE140, HIS163, GLU166, and GLN189 receptors, with bond lengths of 2.52 Å, 2.17 Å, 1.89 Å, and 2.18 Å, respectively. Additionally, it forms pi-alkyl interactions with CYS145 receptors, with bond lengths of 2.78 Å.

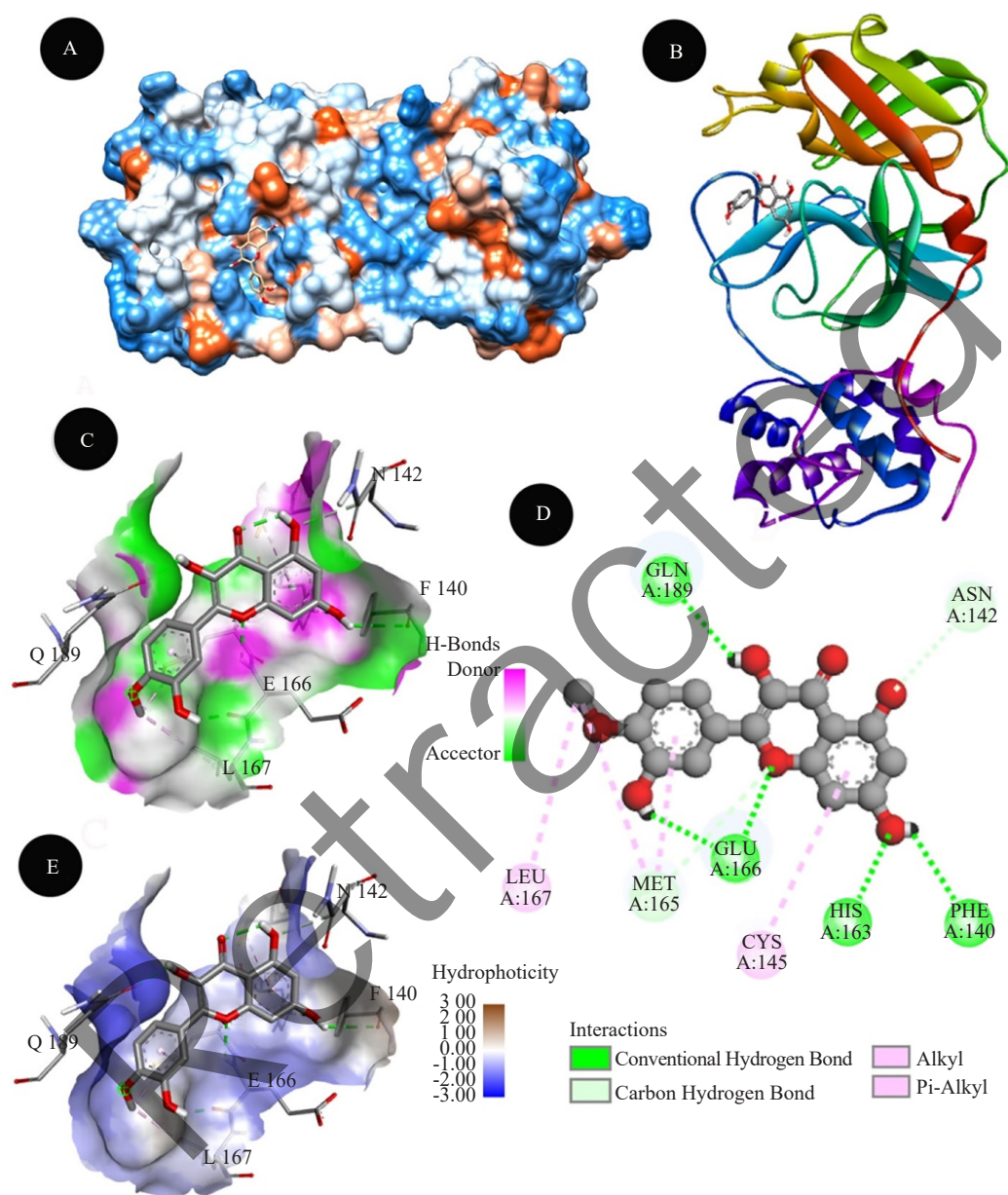


Figure 10. Docking analysis of SARS-CoV-2 M^{pro} binding with Tamarixetin (A) hydrophobicity surface 3D representation (B) 3D representation of Tamarixetin with SARS-CoV-2 M^{pro} interaction (C) Interactions of Tamarixetin through H-bond in a pocket site of SARS-CoV-2 M^{pro} (D) 2D representation of Tamarixetin in active site of SARS-CoV-2 M^{pro} (E) Interactions of Tamarixetin through hydrophobic bond in a pocket site of SARS-CoV-2 M^{pro}

Figure 11 demonstrates 6-Deacetylnimbin, which is involved in one conventional hydrogen bond with the GLU166 receptor, while other active residual sites show interactions with attractive charges on HIS163 and HIS172. It also forms a carbon-hydrogen bond interaction with the GLN189 receptor, with a bond length of 3.32 Å.

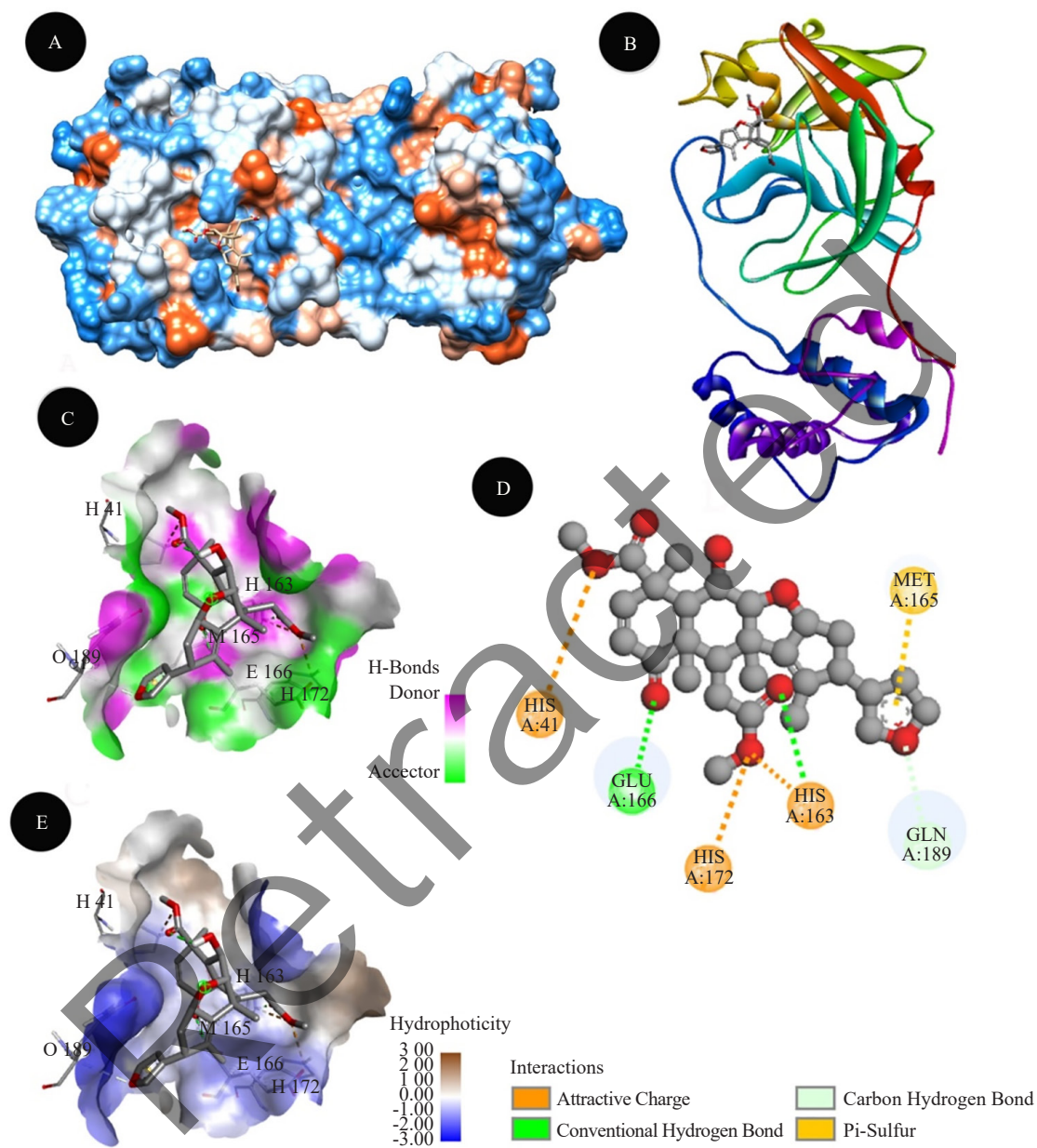


Figure 11. Docking analysis of SARS-CoV-2 M^{pro} binding with 6-Deacetylnimbin (A) hydrophobicity surface 3D representation (B) 3D representation of 6-Deacetylnimbin with SARS-CoV-2 M^{pro} interaction (C) Interactions of 6-Deacetylnimbin through H-bond in a pocket site of SARS-CoV-2 M^{pro} (D) 2D representation of 6-Deacetylnimbin in active site of SARS-CoV-2 M^{pro} (E) Interactions of 6-Deacetylnimbin through hydrophobic bond in a pocket site of SARS-CoV-2 M^{pro}

Nimbolide in Figure 12 exhibits two conventional hydrogen bonds with ASN142 and GLY143 receptors, with bond lengths of 2.82 Å and 1.81 Å, respectively. It also forms carbon-hydrogen bonds with the PHE140 and GLU166 receptors, with bond lengths of 2.76 Å and 2.83 Å, respectively, as well as pi-alkyl interactions with the CYS145 and HIS163 receptors, with bond lengths of 4.02 Å and 5.31 Å, respectively.

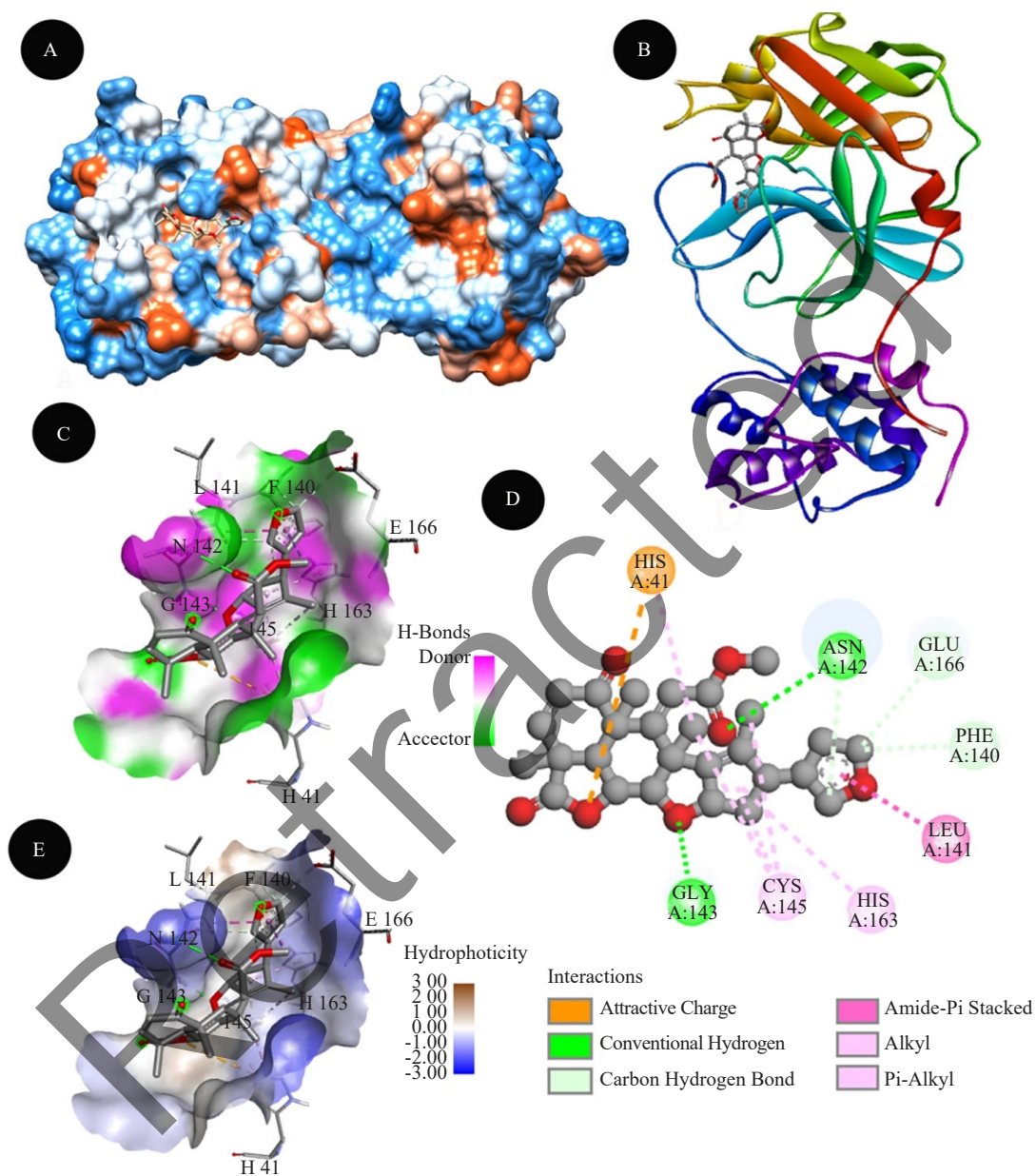


Figure 12. Docking analysis of SARS-CoV-2 M^{pro} binding with Nimbolide (A) hydrophobicity surface 3D representation (B) 3D representation of Nimbolide with SARS-CoV-2 M^{pro} interaction (C) Interactions of Nimbolide through H-bond in a pocket site of SARS-CoV-2 M^{pro} (D) 2D representation of Nimbolide in active site of SARS-CoV-2 M^{pro} (E) Interactions of Nimbolide through hydrophobic bond in a pocket site of SARS-CoV-2 M^{pro}

Figure 13 demonstrates Tricin which displays three similar bond patterns compared to Remdesivir, involving CYS145, HIS163, and GLU166 receptors with additional ASN142 with bond lengths of 3.82 Å, 2.18 Å, 2.52 Å, and 3.32 Å respectively. It also forms carbon hydrogen bonds with the THR190 receptor with bond lengths of 2.14 Å.

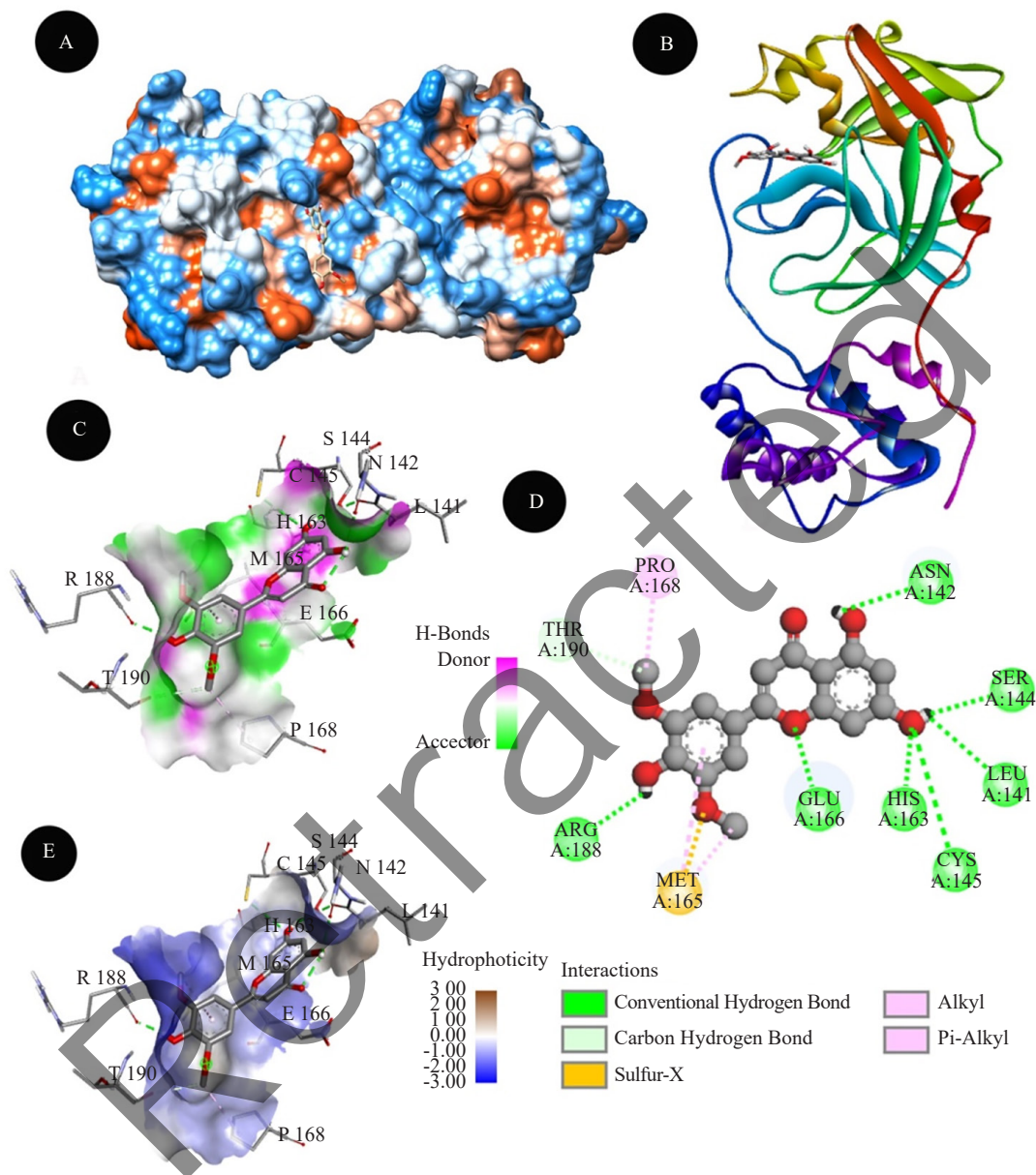


Figure 13. Docking analysis of SARS-CoV-2 M^{pro} binding with Tricin (A) hydrophobicity surface 3D representation (B) 3D representation of Tricin with SARS-CoV-2 M^{pro} interaction (C) Interactions of Tricin through H-bond in a pocket site of SARS-CoV-2 M^{pro} (D) 2D representation of Tricin in active site of SARS-CoV-2 M^{pro} (E) Interactions of Tricin through hydrophobic bond in a pocket site of SARS-CoV-2 M^{pro}

3.1.2 Pharmacokinetic predictive studies

The compound's water solubility ($\log S$) indicates its solubility in water at 25 °C. It's expressed as the logarithm of the molar concentration ($\log \text{ mol/L}$), providing the predicted water solubility of the compound, Remdesivir, Sideroxylonal C, Epigallocatechin gallate (EGCG), Tricin, Luteolin, Ombuin, 6-Deacetylningbin, Coriandron, Epicatechin shows similar values. While, Tamarixetin has a lower value and Nobiletin, Tangeretin and Nimbolide possess higher values than the control drug. Caco-2 permeability is considered to be high in Remdesivir $>6 \times 10^8$ cm/s. The lowest values were found in Tangeretin 0.02×10^8 , while among all the natural drugs, the highest values were noted in Ombuin $>4 \times 10^8$. The intestine serves as the main site for drug absorption from an orally administered solution. A molecule exhibiting intestinal absorption of less than 30% is deemed to be poorly absorbed. Tables 3-6 show all the natural drugs potentially highly absorbed in the intestinal absorption studies. The model determines whether a specific compound is prone to being a substrate of P-glycoprotein. It consistently predicts affirmation in this regard in Tamarixetin, Tricin, Luteolin, Ombuin, 6-Deacetylningbin, Coriandron, Epicatechin and EGCG. While, negative in Nobiletin, Tangeretin, Nimbolide and Coriandron-A. P-glycoprotein I & II inhibitors are negative in Tamarixetin, Tricin, Luteolin, Ombuin, 6-Deacetylningbin, Coriandron, and Epicatechin. While, Sideroxylonal C, Nobiletin, Tangeretin, and Nimbolide act as P-glycoprotein I & II inhibitors. A compound with a $\log K_p$ greater than -2.5 is deemed to exhibit relatively low skin permeability. This suggests that all compounds might hold promise for advancing transdermal drug delivery. The volume of distribution (VD) represents the theoretical volume necessary for a drug to achieve uniform distribution in the bloodstream. Based on Tables 3-6 and typical benchmarks Remdesivir, Sideroxylonal C, Tricin, Epigallocatechin gallate (EGCG), Ombuin, Coriandron, Nobiletin, Tangeretin, Nimbolide exhibits a low VD, while Tamarixetin, Luteolin, 6-Deacetylningbin and Epicatechin demonstrates a high VD. The Fraction Unbound parameter anticipates the proportion that will remain unbound in plasma, as illustrated by the values in Tables 3-6. Understanding a drug's capacity to penetrate the brain is crucial for minimizing adverse effects and toxicities. When a drug's $\log \text{ BBB}$ (Blood-Brain Barrier permeability coefficient) exceeds -0.6 in Nimbolide and -0.082 in Corindron, it's likely to effectively cross the BBB, whereas molecules with $\log \text{ BBB}$ values exceeding -1 tend to distribute poorly in the brain. Another metric to consider is the blood-brain permeability-surface area product, also known as CNS Permeability. Compounds with a $\log \text{ PS} > -2$ can enter the Central Nervous System (CNS), whereas those with $\log \text{ PS} < -3$ cannot penetrate the CNS. In the present study, it is anticipated that Luteolin and Nimbolide will penetrate the CNS from the rest of the natural drugs. Cytochrome P450 stands as a pivotal enzyme for detoxification within the body, playing a crucial role in deactivating numerous drugs through its isoforms, although it can also activate certain ones. This is evident from Tables 3-6. Drug clearance is the result of both hepatic and renal processes, with renal clearance involving excretion through the kidneys and closely linked to bioavailability. The anticipated Total Clearance for all drugs is provided in $\log (\text{ ml/min/kg})$. Additionally, the forecasts suggest that none of all the drugs are likely to inhibit hERG I. However, the scenario may vary concerning hERG II, as shown in Tables 3-6. Remdesivir, Sideroxylonal C, and EGCG inhibit hERG II, whereas the rest of other drugs do not. The LD50 values, a standard gauge of acute toxicity, represent the dosage at which 50% of test animals succumb to a compound. These values are determined using the ORAT and ORCT indices, with predicted measurements provided in mol/kg . Drug-induced liver injury poses a significant safety challenge in pharmaceutical development. Hepatotoxicity arises from the disturbance of liver function, and positive predicted values are observed only for synthetic drug Remdesivir. However, the projected outcomes for Skin Sensitisation indicate negativity. *T. Pyriformis*, a protozoan bacterium commonly employed in toxicity assessments, exhibits consistent predicted values for this parameter across all the drugs in Tables 3-6.

Table 3. ADMET predictive study of Remdesivir, Tamarixetin, Sideroxylonal C, Tricin, and Epigallocatechin gallate (EGCG)

	Remdesivir	Tamarixetin	Sideroxylonal C	Tricin	EGCG	
	Water solubility (log mol/L)	-3.07	-3.007	-3.374	-3.276	-2.894
	CaCO ₂ permeability (log Papp in 10 ⁻⁶ cm/s)	0.635	0.002	0.189	0.12	1.521
	Intestinal absorption (% absorbed)	71.109	73.005	69.918	89.713	47.395
Absorption	Skin permeability (log Kp)	-2.735	-2.735	-2.735	-2.735	-2.735
	P-glycoprotein substrate	Yes	Yes	Yes	Yes	Yes
	P-glycoprotein I inhibitor	Yes	No	Yes	No	No
	P-glycoprotein II inhibitor	No	No	Yes	No	Yes
	VDss (human) (log L/kg)	0.307	1.089	0.238	0.798	0.806
Distribution	Fraction unbound (human) (Fu)	0.005	0.089	0	0.084	0.215
	BBB permeability (logBB)	-2.056	-1.161	-1.564	-1.115	-2.184
	CNS permeability (logPS)	-4.675	-3.172	-3.159	-3.411	-3.96
	CYP2D6 substrate	No	No	No	No	No
	CYP3A4 substrate	Yes	No	Yes	No	No
	CYP1A2 inhibitor	No	Yes	No	Yes	No
Metabolism	CYP2C19 inhibitor				Yes	No
	CYP2C9 inhibitor	No	No	No	No	No
	CYP2D6 inhibitor	No	No	No	No	No
	CYP3A4 inhibitor	No	No	No	No	Yes
	Total clearance (log ml/min/kg)	0.198	0.508	0.02	0.62	0.292
Excretion	Renal OCT2 substrate	No	No	No	No	No
	Max. tolerated dose (human) (log mg/kg/day)	0.15	0.577	0.439	0.351	0.441
	hERG I inhibitor	No	No	No	No	No
	hERG II inhibitor	Yes	No	Yes	No	Yes
	Oral rat acute toxicity (LD50) (mol/kg)	2.043	2.407	2.746	2.229	2.522
Toxicity	Oral rat chronic toxicity (LOAEL) (log mg/kg bw/day)	1.639	2.476	3.272	1.82	3.065
	Hepatotoxicity	Yes	No	No	No	No
	Skin sensitization	No	No	No	No	No
	<i>Tetrahymena pyriformis</i> toxicity (µg/L)	0.285	0.299	0.285	0.329	0.285
	Minnow toxicity (mM)	0.291	2.289	2.592	1.754	7.713

Table 5. ADMET predictive study of Remdesivir, Nobiletin, Tangeretin and Coriandron

	Remdesivir	Nobiletin	Tangeretin	Coriandron-A	
	Water solubility (log mol/L)	-3.07	-4.949	-4.792	-3.131
	CaCO ₂ permeability (log Papp in 10 ⁻⁶ cm/s)	0.635	1.306	1.245	1.168
	Intestinal absorption (% absorbed)	71.109	98.921	98.478	96.14
Absorption	Skin permeability (log Kp)	-2.735	-2.715	-2.678	-3.343
	P-glycoprotein substrate	Yes	No	No	No
	P-glycoprotein I inhibitor	Yes	Yes	Yes	No
	P-glycoprotein II inhibitor	No	Yes	Yes	No
	VDss (human) (log L/kg)	0.307	0.281	0.226	0.143
Distribution	Fraction unbound (human) (Fu)	0.005	0.179	0.188	0.363
	BBB permeability (logBB)	-2.056	-1.254	-1.026	-0.082
	CNS permeability (logPS)	-4.675	-3.142	-3.011	-2.878
	CYP2D6 substrate	No	No	No	No
	CYP3A4 substrate	Yes	Yes	Yes	Yes
	CYP1A2 inhibitor	No	Yes	Yes	No
Metabolism	CYP2C19 inhibitor	No	Yes	Yes	No
	CYP2C9 inhibitor	No	Yes	Yes	No
	CYP2D6 inhibitor	No	No	No	No
	CYP3A4 inhibitor	No	Yes	Yes	No
	Total clearance (log ml/min/kg)	0.198	0.789	0.78	0.841
Excretion	Renal OCT2 substrate	No	No	No	No
	Max. tolerated dose (human) (log mg/kg/day)	0.15	0.443	0.385	0.348
	hERG I inhibitor	No	No	No	No
	hERG II inhibitor	Yes	No	No	No
	Oral Rat acute toxicity (LD50) (mol/kg)	2.043	2.459	2.368	2.287
Toxicity	Oral rat chronic toxicity (LOAEL) (log mg/kg bw/day)	1.639	0.82	0.944	2.002
	Hepatotoxicity	Yes	No	No	No
	Skin sensitization	No	No	No	No
	<i>Tetrahymena pyriformis</i> toxicity (µg/L)	0.285	0.315	0.355	0.728
	Minnow toxicity (mM)	0.291	0.686	0.144	1.2

Table 6. ADMET predictive study of Remdesivir, Nimbolide, Epicatechin

	Remdesivir	Nimbolide	Epicatechin	
	Water solubility (log mol/L)	-3.07	-5.166	-3.117
	CaCO ₂ permeability (log Papp in 10 ⁻⁶ cm/s)	0.635	0.92	0.283
	Intestinal absorption (% absorbed)	71.109	100	68.829
Absorption	Skin permeability (log Kp)	-2.735	-3.599	-2.735
	P-glycoprotein substrate	Yes	No	Yes
	P-glycoprotein I inhibitor	Yes	Yes	No
	P-glycoprotein II inhibitor	No	Yes	No
	VDss (human) (log L/kg)	0.307	0.028	1.027
Distribution	Fraction unbound (human) (Fu)	0.005	0.043	0.235
	BBB permeability (logBB)	-2.056	-0.675	-1.054
	CNS permeability (logPS)	-4.675	-2.658	-3.298
	CYP2D6 substrate	No	No	No
	CYP3A4 substrate	Yes	Yes	No
	CYP1A2 inhibitor	No	No	No
Metabolism	CYP2C19 inhibitor		No	No
	CYP2C9 inhibitor	No	No	No
	CYP2D6 inhibitor	No	No	No
	CYP3A4 inhibitor	No	No	No
	Total clearance (log ml/min/kg)	0.198	0.249	0.183
Excretion	Renal OCT2 substrate	No	No	No
	Max. tolerated dose (human) (log mg/kg/day)	0.15	-0.476	0.438
	hERG I inhibitor	No	No	No
	hERG II inhibitor	Yes	No	No
	Oral rat acute toxicity (LD50) (mol/kg)	2.043	2.374	2.428
Toxicity	Oral rat chronic toxicity (LOAEL) (log mg/kg bw/day)	1.639	1.554	2.5
	Hepatotoxicity	Yes	No	No
	Skin sensitization	No	No	No
	<i>Tetrahymena pyriformis</i> toxicity (µg/L)	0.285	0.328	0.347
	Minnnow toxicity (mM)	0.291	0.318	3.585

4. Discussion

COVID-19, an infectious ailment with rapid transmission, prompted the WHO to issue technical guidelines and advisories for public safety.³⁵ Presently, approved medications and expedited vaccination programs aim to curb its spread. Augmenting modern treatments, Ayurvedic therapies enhance immunity and aid in disease prevention. Thus, this study endeavors to identify phytoconstituents capable of combating the disease. Among twelve markers, Tamarixetin exhibits efficacy comparable to synthetic drugs. Both drugs target six active residual sites on the viral protein, with Tamarixetin displaying a bond pattern akin to the control drug. Conventional hydrogen bonds were observed at four sites viz. PHE140, HIS163, GLU166, and GLN189 with bond lengths of 2.52, 2.17, 1.89, and 2.18 Å, respectively. Additionally, a carbon-hydrogen bond was found at ASN 142, while an alkyl & pi-alkyl bond was identified at CYS 145. These findings suggest that Tamarixetin can complement synthetic medication in treating COVID-19.

5. Conclusion

A persistent mutation within the virus strain presents a public safety concern. In contrast, the Ayurvedic medicinal system seeks to complement conventional therapies, playing a crucial role in battling the disease and fortifying the immune system. This approach empowers individuals to resist future virus strains effectively. Recent studies strongly endorse the natural phytomarker, Tamarixetin, underscoring its pivotal role in drug receptor interactions. Tamarixetin engages with four carbon-hydrogen bonds within the 6LU7 M^{pro} protein, resembling the action of Remdesivir, a standard treatment, on similar active sites (PHE 140, ASN 142, CYS 145, GLU 166, ALN 189). Consequently, this inquiry establishes a sturdy groundwork for developing new drugs to counteract the spreading mutation. Nonetheless, to enhance the credibility of the research, it requires clinical investigation and validation.

Acknowledgments

It is our pleasure to express our gratitude to Mr. Hardik Ukani (Managing Director) Vasu Health Care Pvt. Ltd. for providing research lab facilities and always encouraging us to come up with new innovations that could help and benefited to humanity. Author would like to extend their thanks to Vasu Research centre team & Vasu Health Care Pvt Ltd (Vasudhars) for their assistance and kind support at every stage.

Conflict of interest

Authors declare there is no conflict of interest at any point with reference to research findings.

References

- [1] World Health Organization (WHO). <https://covid19.who.int/table> (accessed August 5, 2020).
- [2] World Health Organization (WHO). <http://www.who.int/emergencies/diseases/novel-coronavirus-2019/situation-reports/> (accessed August 5, 2020).
- [3] Huang, C.; Wang, Y.; Li, X.; Ren, L.; Zhao, J.; Hu, Y.; Zang, L.; Fan, G.; Xu, J.; Gu, X.; Cheng, Z. *Lancet*. **2020**, *395*, 497-506.
- [4] Chen, N.; Zhou, M.; Dong, X.; Qu, J.; Gong, F.; Han, Y.; Qui, Y.; Wang, J.; Liu, Y.; Wei, Y.; Yu, T. *Lancet*. **2020**, *395*, 507-513.
- [5] Chan, J. F. W.; Yuan, S.; Kok, K. H.; To, K. K. W.; Chu, H.; Yang, J.; Xing, F.; Liu, J.; Yip, C. C. Y.; Poon, R. W. S.; Tsoi, H. W. *Lancet*. **2020**, *395*, 514-523.
- [6] Gorbalenya, A. E.; Baker, S. C.; Baric, R. S.; de Groot, R. J.; Drosten, C.; Gulyaeva, A. A.; Haagmans, B. L.; Lauber, C.; Leontovich, A. M.; Neuman, B. W.; Penzar, D. Severe acute respiratory syndrome-related Corona virus: the species and its viruses-a statement of the Corona virus Study Group. *bioRxiv*. **2020**, *11*, 1-15.

- [7] Schoeman, D.; Fielding, B. C. *Viol. J.* **2019**, *16*, 1-22.
- [8] Bradwell, K.; Combe, M.; Domingo-Calap, P.; Sanjuán, R. *Genetics.* **2013**, *195*, 243-251.
- [9] Bisgaard, T.; Warltier, D. C. *J. Am. Soc. Anesthesiol.* **2006**, *104*, 835-846.
- [10] Liu, J. Z.; Huang, Y. H.; Hand, P. J. *Acupunct. Electrother. Res.* **1988**, *13*, 9-23.
- [11] Horby, P.; Lim, W. S.; Emberson, J.; Mafham, M.; Bell, J.; Linsell, L.; Staplin, N.; Brightling, C.; Ustianowski, A.; Elmahi, E.; Prudon, B. Effect of dexamethasone in hospitalized patients with COVID-19-preliminary report. *MedRxiv.* **2020**, 1-24.
- [12] Warren, T.; Jordan, R.; Lo, M.; Soloveva, V.; Ray, A.; Bannister, R. *Open Forum Infect. Dis.* **2015**, *2*, LB-2.
- [13] Beigel, J. H.; Tomashek, K. M.; Dodd, L. E.; Mehta, A. K.; Zingman, B. S.; Kalil, A. C.; Hohmann, E.; Chu, H. Y.; Luetkemeyer, A.; Kline, S.; de Castilla, D. L. *New Eng. J. Med.* **2020**, *383*, 1-11.
- [14] National Institute of Health (NIH) (gov). <https://www.covid19treatmentguidelines.nih.gov/therapies/antivirals-including-antibody-products/remdesivir/> (accessed January 2, 2024).
- [15] Tett, S.; Cutler, D.; Day, R. *Baillieres clin. Rheumatol.* **1990**, *4*, 467-489.
- [16] Schentag, J. J.; Ballow, C. H. *Am. J. Med.* **1991**, *91*, S5-S11.
- [17] Bahal, N.; Nahata, M. C. *Ann. Pharmacother.* **1992**, *26*, 46-55.
- [18] Arshad, S.; Kilgore, P.; Chaudhry, Z. S.; Jacobsen, G.; Wang, D. D.; Huitsing, K.; Brar, I.; Alangaden, G. J.; Ramesh, M. S.; McKinnon, J. E.; O'Neill, W. *Int. J. Infect. Dis.* **2020**, *97*, 396-403.
- [19] Vanzara, A.; Patel, R.; Patel, A.; Patel, N.; Yadav, K.; Nagar, P. J. *Infect. Dis. Pre. Med.* **2021**, *10*, 267.
- [20] Rastogi, S.; Pandey, D.; Singh, R. J. *Ayurveda Integr. Med.* **2020**, *13*, 100312.
- [21] Salzberger, B.; Glück, T.; Ehrenstein, B. *Infection.* **2020**, *48*, 151-153.
- [22] Ren, J. L.; Zhang, A. H.; Wang, X. J. *Pharm. Res.* **2020**, *155*, 104743.
- [23] Gui-Qiang, W.; Lie, Z.; Xia, W.; Yan-Mei, J.; Fu-Sheng, W. *Infect. Dis. Immun.* **2021**, *1*, 17-19.
- [24] Jin, Z.; Du, X.; Xu, Y.; Deng, Y.; Liu, M.; Zhao, Y.; Zhang, B.; Li, X.; Zhang, L.; Peng, C.; Duan, Y. *Nature.* **2020**, *582*, 289-293.
- [25] Lipinski, C. A.; Lombardo, F.; Dominy, B. W.; Feeney, P. J. *Adv. Drug Deliv. Rev.* **2012**, *23*, 3-25.
- [26] SWISSADME, Swiss Institute of Bioinformatics. <http://www.swissadme.ch/> (accessed August 5, 2020).
- [27] Zhang, L.; Lin, D.; Sun, X.; Curth, U.; Drosten, C.; Sauerhering, L.; Becker, S.; Rox, K.; Hilgenfeld, R. *Science.* **2020**, *368*, 409-412.
- [28] Jin, Z.; Du, X.; Xu, Y.; Deng, Y.; Liu, M.; Zhao, Y.; Zhang, B.; Li, X.; Zhang, L.; Peng, C.; Duan, Y. *Nature.* **2020**, *582*, 289-293.
- [29] Wang, M.; Cao, R.; Zhang, L.; Yang, X.; Liu, J.; Xu, M.; Shi, Z.; Hu, Z.; Zhong, W.; Xiao, G. *Cell Res.* **2020**, *30*, 269-271.
- [30] Andrade, B. S.; Ghosh, P.; Barh, D.; Tiwari, S.; Silva, R. J. S.; de Assis Soares, W. R.; Melo, T. S.; Freitas, A. S.; González-Grande, P.; Palmeira, L. S.; Alcantara, L. C. J. *F1000 Research.* **2020**, *9*, 514.
- [31] Patel, R.; Vanzara, A.; Patel, N.; Vasava, A.; Patil, S.; Rajput, K. *Coronaviruses.* **2021**, *8*, 1
- [32] Morris, G. M.; Huey, R.; Lindstrom, W.; Sanner, M. F.; Belew, R. K.; Goodsell, D. S.; Olson, A. J. *J. Comput. Chem.* **2009**, *30*, 2785-2791.
- [33] Schrodinger, LLC. *The PyMOL Molecular Graphics System, Version 1.8.* Schrodinger, LLC; New York, NY: USA, 2015.
- [34] Pires, D. E.; Blundell, T. L.; Ascher, D. B. *J. Med. Chem.* **2015**, *58*, 4066-4072.
- [35] World Health Organization (WHO). <https://www.who.int/emergencies/diseases/novel-coronavirus-2019/advice-for-public> (accessed August 5, 2020).